EFFECTS OF $q(r)$ ON THE ALPHA PARTICLE RIPPLE LOSS IN TFTR

S.J. ZWEBEN, D.S. DARROW, S.H. BATHA*, R.V. BUDNY, M. DIESSO,
H.W. HERRMANN, J. GIARRUSSO, M.H. REDI, H. TAKAHASHI,
S. VON GOELER, R.B. WHITE, R.M. WIELAND
Princeton Plasma Physics Laboratory,
Princeton University,
Princeton, New Jersey,
United States of America

* Fusion Physics and Technology,
Torrance, California,
United States of America

ABSTRACT. An experiment was done with TFTR DT plasmas to measure the effect of the $q(r)$ profile on the alpha particle ripple loss using a radially movable scintillator detector 20° below the outer midplane. The experimental results were compared with toroidal field (TF) ripple loss calculations done using a Monte Carlo guiding centre orbit following code (ORBIT). Although some of the experimental results are consistent with the ORBIT code modelling, the measured variation of the alpha particle loss with $q(r)$ could not be explained by this code. This inconsistency is most likely due to the effect of limiter shadowing on alpha particle diffusion into this detector, which cannot be modelled with ORBIT.

1. INTRODUCTION

The aim of the experiment performed was to test the predicted $q(r)$ dependence of the standard theory for toroidal field (TF) ripple induced 'stochastic ripple diffusion' (SRD) using deuterium–tritium (DT) alpha particles in TFTR. According to the original SRD model [1], trapped alpha particles will rapidly diffuse when their 'banana tips' fall in a region where the TF ripple is larger than

$$\delta_{\mathrm{GWB}} \approx (\varepsilon/N\pi q)^{3/2}(1/\rho q'). \quad (1)$$

Here δ_{GWB} is the Goldston–White–Boozer (GWB) stochastic threshold (δ is the peak to average $\delta B_{\mathrm{tor}}/B_{\mathrm{tor}}$ along a field line), $\varepsilon = r/R$ is the location of the ion's banana tip (where the orbit is most sensitive to the TF ripple perturbation), N is the number of TF coils, ρ is the gyroradius of the orbit, and q and q' $(= \partial q/\partial r)$ depend on the magnetic $q(r)$ profile at the banana tip.

When this stochasticity condition is satisfied, the alpha particle banana tip locations become decorrelated between successive bounces, causing the orbit to diffuse radially until it leaves the stochastic region or hits the wall. Note that this SRD of banana orbits is fundamentally different from ripple trapping, which occurs only when an ion is trapped in the local magnetic well between two TF coils. The SRD process occurs for trapped fast ions over a wide range of pitch angles, whereas ripple trapping occurs only for a small range of pitch angles nearly perpendicular to the toroidal field.

Although there were several simplifying assumptions used in deriving Eq. (1), a fundamental feature of this model is that the SRD threshold depends on the $q(r)$ profile, which determines the stochasticity condition of the banana orbit tip. The result of Eq. (1) has recently been generalized to include non-circular equilibria, but the sensitivity of the SRD mechanism to the $q(r)$ profile remains [2]. This sensitivity to $q(r)$ may be important in the 'advanced' tokamak regime at $q(0) > 1$, where the stochastic threshold is lower than it is for $q(0) < 1$, and the alpha particle loss due to TF ripple is predicted to be relatively high [3].

Experimental studies have previously been made of the effects of TF ripple on fast ion confinement in tokamaks [4]. For example, the heating of the outer wall due to ripple trapping and loss of 90 keV deuterium beam ions was measured in JT-60U [5], and good agreement was found between the heating pattern and the orbit following Monte Carlo (OFMC) calculations. Ripple transport experiments have also been done in JET using 1 MeV triton burnup [6], in Tore Supra using a calorimeter detector to measure the loss of ≈200 keV minority ion cyclotron resonance heated (ICRH) tail ions [7], and

in TFTR using the pellet charge exchange analyser of confined alpha particles (PCX) [8]. Although these experimental results generally confirmed the modelling of TF ripple diffusion and loss, none of them specifically tested the $q(r)$ profile dependence of the SRD mechanism. Although two experiments have recently inferred an increased fast ion loss at high $q(0)$, one using triton burnup on JT-60U [9] and another using neutron emission from the fusion of deuterium and tritium beam ions in TFTR [10], no measurements of the fast ion loss to the wall were made.

The present experiment was based on a fast ion scintillator detector previously used for deuterium–deuterium (DD) fusion products in TFTR [11, 12]. This detector is located where the SRD loss was expected, just below the outer midplane (in the ion ∇B drift direction). The previous DD results showed several characteristics expected for fusion product loss induced by SRD; in particular, the measured pitch angle distribution peaked near the expected angle for SRD (which was significantly larger than that for first orbit loss), and the total fusion product loss fraction (per DD neutron) varied with plasma current in a similar way to predictions from the simplified collisionless MAPLOS (bounce mapping) code [11]. The radial diffusion of DD fusion products was also measured in the shadow of both the outer limiter and a second movable probe, and the inferred radial step sizes were similar to those predicted by the collisionless GWB model [12].

A survey of the DT alpha particle loss measured by this midplane detector has been presented previously [13]. The main trends in the data were:

(a) For a given type of plasma, the DT and DD fusion product loss fractions (per neutron) were similar, as expected from the SRD model (Eq. (1)), since their gyroradii are similar.

(b) The DT alpha particle loss per neutron peaked at a plasma current of $I = 1.0$ MA, almost as expected from the collisionless MAPLOS calculations.

(c) Between $I = 1$ MA and $I = 2$ MA the pitch angle of the measured loss was roughly consistent with the MAPLOS calculation of TF ripple loss.

(d) The alpha particle loss signal at $I = 2.0$ MA varied by a factor of ≈20 when the detector aperture was moved ±1.5 cm radially near the outer limiter, and the pitch angle distribution varied considerably over this range.

The present article describes an experiment for measuring the $q(r)$ dependence of the alpha particle ripple loss in TFTR, and an attempt using the ORBIT guiding centre code (which is more accurate than the MAPLOS code) to understand the data obtained. The experimental design is described in Section 2, the detector and limiter geometry is reviewed in Section 3 and the ORBIT model is described in Section 4. The experimental results are compared with the ORBIT code in Section 5, the limiter shadowing effect is described in Section 6, and the results are discussed and conclusions are drawn in Section 7.

2. EXPERIMENTAL DESIGN

The experiment was designed to vary the quantity $q^{3/2}q'\rho$ in Eq. (1), which determines the SRD threshold. The plasma size was kept fixed at the standard major and minor radii of $R_0 = 2.52$ m and $a = 0.87$ m, as used for the previous study of first orbit alpha particle loss to the vessel bottom [14]. The baseline plasma parameters were $I = 1.4$ MA, $B_0 = 4.7$ T and 7.5 MW of NBI (one tritium beam and two deuterium beams), where B_0 was measured at R_0.

Three plasma scans were done to vary the SRD threshold as widely as possible around this baseline. These scans were:

(a) A '$q(r)$ *scan*' done by ramping up or down the plasma current before NBI, as illustrated in Fig. 1. The rampdown from $I = 2.2$ MA to 1.4 MA produced a relatively high current density and low $q(r)$ in the plasma core, while the rampup from $I = 0.6$ MA to 1.4 MA produced a low current density and high $q(r)$ in the core. The higher $q(r)$ for the rampup case should reduce the SRD threshold and increase the ripple loss, and vice versa.

(b) A '$q(a)$ *scan*' at a constant $I = 1.4$ MA with toroidal fields of $B_0 = 4.7$, 3.9 and 3.4 T. This scan decreased both q and q' with decreasing B_0, which should increase the stochastic ripple threshold and decrease the ripple loss, from Eq. (1). The increased ρ with decreasing B_0 only partially offsets the expected increase in the SRD threshold.

(c) A 'ρ *scan*' at fixed $q(a)$ with toroidal fields of $B_0 = 4.7$, 3.9 and 3.4 T at plasma currents of $I = 1.4$, 1.15 and 1.0 MA, respectively. This scan varied the alpha particle gyroradius ρ at a nearly fixed $q(r)$. The stochastic ripple threshold should decrease and the

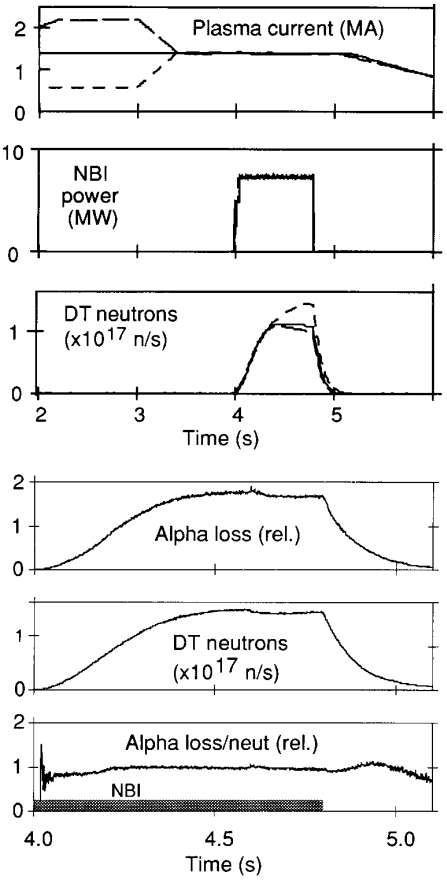

FIG. 1. Typical time evolution of the plasmas in this experiment. The top frame shows the current versus time for three shots in the $q(r)$ scan: one in which the plasma current was 'ramped up', one in which it was 'ramped down', and one in which it was 'straight across'. The 7.5 MW of NBI was applied after the current ramps when all the plasmas were at $I = 1.4$ MA. The lower frames show a typical time dependence of the alpha particle loss, measured just below the outer midplane, which follows the DT neutron rate closely. This near constancy of the alpha particle loss per DT neutron rate during NBI was observed for all the plasmas in this experiment.

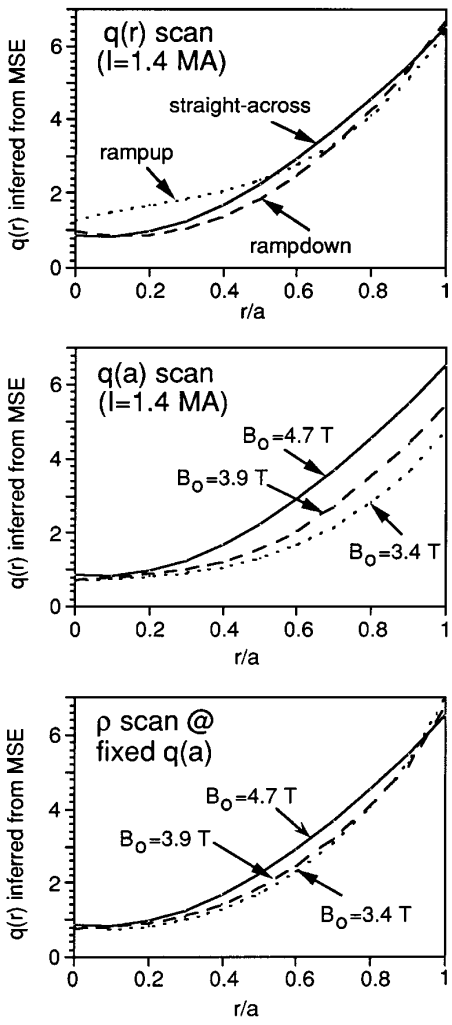

FIG. 2. Variation of the $q(r)$ profiles measured by MSE for the three different plasma scans in this experiment. Common to all three scans is the 'baseline' shot at $I = 1.4$ MA and $B_0 = 4.7$ T (the 'straight across' case of Fig. 1). The '$q(r)$ scan' is produced by current ramping, the '$q(a)$ scan' by varying the toroidal field at a fixed current ($I = 1.4$ MA) and the 'ρ scan' by varying the I and B_0 together at a constant $q(a)$.

ripple loss should increase with decreasing B from Eq. (1).

The actual $q(r)$ profiles for typical plasmas in these scans are shown in Fig. 2, based on motional Stark effect (MSE) measurements of the pitch angle of the magnetic field [15, 16]. Analytic fits to these $q(r)$ profiles were used in the ORBIT modelling. The plasma parameters were nearly constant during these scans, as listed in Table I. There was very little coherent MHD activity in these low powered discharges and no perceptible coherent MHD-induced alpha particle loss. At low $q(a)$ there were sawteeth, but these did not significantly affect the time averaged alpha particle loss rate. A full description of the details concerning the experimental design and plasma conditions is given in Ref. [17].

Table I. Plasma Parameters
(at 4.5 to 4.8 s during NBI)

$R_0 = 2.52$ m (centre of outermost flux surface)
$a = 0.87$ m (minor radius from R_0)
$I = 1.4$ to 1.0 MA (during NBI)
$B_0 = 4.7$ to 3.4 T (as measured at R_0)
$P_{\rm NBI} = 7.5$ MW (one tritium beam and two deuterium beams)
$n_{\rm e}(0) = (3.0 \pm 0.5) \times 10^{13}$ cm^{-3}
$T_{\rm e}(0) = 5.5 \pm 0.5$ keV
$T_{\rm i}(0) = 12.5 \pm 2.5$ keV
$\langle \tau_{\alpha,E} \rangle \approx 0.1$ s (average alpha particle energy e-folding time)
$\langle \tau_{\perp,90^\circ} \rangle \approx 10$ s (average alpha particle 90° pitch angle scattering time)
$\langle Z_{\rm eff} \rangle \approx 3$

The size of the SRD regions also depends on the TF ripple strength, which is given by a fit to the TFTR magnetic design specification,

$$\delta(\text{peak to average}) = 6 \times 10^{-6} \exp\{[(R - 2.25)^2 + 1.31z^2]^{1/2}/0.166\} \quad (2)$$

where R is the major radius (in metres) and z is the height above the midplane (TFTR is symmetrical about the midplane). This is a slightly improved fit to that used previously [11]. The outer midplane plasma edge is at $R = R_0 + a = 3.39$ m, and the outer midplane limiter location is at $R = R_{\rm lim} + a_{\rm lim} = 3.60$ m. Therefore, the TF ripple is $\delta \approx 0.5\%$ at the midplane plasma edge ($z = 0$), $\delta \approx 2\%$ at the midplane outer limiter and $\delta \approx 0.3\%$ at the top edge of the plasma ($R = 2.52,\ z = 0.87$).

3. DETECTOR AND LIMITER GEOMETRY

The alpha particle diagnostic for this experiment was a radially movable scintillator detector located about 20° poloidally below the outer midplane (in the ion ∇B drift direction), where the TF ripple loss was expected to peak [11–13]. This detector has been extensively described elsewhere [17–19] and so will only be described briefly here.

The alpha particles enter the detector aperture through a small pinhole (0.07 cm × 0.2 cm), pass through a wider slit (0.07 cm × 1.35 cm) and strike a scintillator screen located inside a light-tight enclosure. This aperture pair separates alpha particles according to their pitch angle χ with respect to the total magnetic field $B_{\rm ap}$ at the detector aperture (where $\chi = 90^\circ$ is perpendicular to $B_{\rm ap}$) and their perpendicular gyroradius at the detector aperture $\rho = (2ME)^{0.5}/qB_{\rm ap}$, such that ρ is a measure of the alpha particle energy E with mass M and charge q. The two dimensional (2-D) scintillator light images are sent through an in-vessel coherent quartz fibreoptic bundle (20 × 20 fibres) to an ex-vessel coherent quartz bundle (50 × 50 fibres) and are digitized by an intensified charge coupled device (CCD) camera system every 33 ms. Thus, the measured quantities are the alpha particle flux versus time through the aperture as a function of the local pitch angle (which determines the magnetic moment) and the local perpendicular gyroradius (which determines the alpha particle energy). The total light from the fibreoptic bundle is also measured by a photomultiplier tube for a faster time response.

The alpha particle perpendicular gyroradius range covered by this detector is $\rho \approx$ 2–12 cm, which includes the $\rho \approx$ 8–11 cm expected for 3.5 MeV alpha particles at the detector. The range of pitch angles covered by this detector is $\chi \approx 40$–85° with respect to the local (co-I directed) total B, which includes the whole range of expected SRD loss, but does not include alpha particles that are trapped in the local ripple wells at angles near $\chi \approx 90^\circ$ (the expected ripple trapped alpha particle loss fraction is negligible). This detector design was optimized for good pitch angle resolution (≈6° FWHM), but not for good perpendicular gyroradius (i.e. energy) resolution, since the energy distribution is naturally broadened by the beam–target Doppler shifts of $\Delta E \approx$ 0.5 MeV. The inferred pitch and perpendicular gyroradius have systematic uncertainties of about ±3° and ±1 cm, respectively, which corresponds to a positional uncertainty of ≈0.1 cm on the surface of the 2.5 cm × 2.5 cm square scintillator.

An important and difficult feature of the present experiment is the effect of the limiter geometry, since most of the alpha particles must diffuse past the geometrical projection or 'shadow' of the outer midplane limiters in order to enter the detector aperture [12, 20]. The most important limiters for this experiment are the 'RF limiters', which are poloidal rings covering ±30° around the outer midplane at toroidal locations between ≈100 and 170° in the counter-I direction from the alpha particle detector. These limiters are all circular with major and minor radii of $R_{\rm lim} = 260.6$ cm and $a_{\rm lim} = 99$ cm and a toroidal extent of about ±25 cm. The toroidal surface through the plasma facing edge of these limiters is defined here as their 'geometrical shadow'. The limiter

alignment uncertainty is about 0.3 cm, and each has a toroidal extent of 50 cm. The first wall is much further outward at $a_{\rm wall} \approx 110$ cm.

The location of the alpha particle detector aperture '$r_{\rm ap}$' is defined with respect to this geometrical limiter shadow. For this experiment the aperture was moved horizontally between $r_{\rm ap} = -2.0$ cm and $r_{\rm ap} = +1.0$ cm, where at $r_{\rm ap} = 0$ cm the pinhole aperture is just at the edge of the limiter shadow ($R = 352.5$ cm and $z = -35.6$ cm). Although at $r_{\rm ap} < 0$ cm the aperture itself is radially inside the geometrical limiter shadow, the alpha particle orbits entering the aperture can still pass outside the limiter shadow at the outer midplane, since the aperture itself is below the midplane. Therefore the limiter shadowing effect can be significant in determining the alpha particle loss to the detector even for the innermost position at $r_{\rm ap} = -2.0$ cm (Section 6).

4. MODELLING OF TF RIPPLE LOSS USING THE ORBIT CODE

The experimental results are compared with modelling done using the ORBIT guiding centre code, another version of which was previously used to model TFTR alpha particle ripple loss [21, 22]. This code calculates alpha particle orbit trajectories in the presence of TF ripple and collisions, and determines the characteristics of the alpha particle loss to the wall, for example, the pitch angle, energy and poloidal angle distributions.

The advantage of this code is that it contains all the physics necessary to accurately describe the stochastic ripple diffusion of alpha particle orbits in TFTR. The main disadvantage of this code is that it assumes that the wall is a smooth toroidal surface, and so does not correctly calculate the effect of the limiter shadowing on the local alpha particle flux to the detector. The strategy of the analysis of Section 5 will be to first compare the experimental results with the ORBIT code modelling and then, since good agreement is not found, to explore the limiter shadowing effect in Section 6.

The inputs to the ORBIT code were fits to the $q(r)$ profiles obtained from the MSE/VMEC equilibrium analysis [15, 16] and the Abel inverted neutron (i.e. alpha particle) source profile shapes measured by the multichannel neutron collimator [23]. These fits are listed in Table 2 of Ref. [17]. To obtain a magnetic equilibrium, the code also inputs the locations

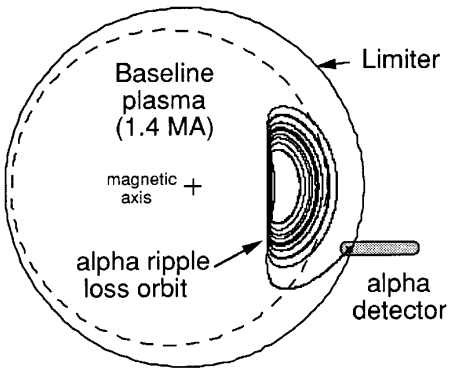

FIG. 3. A typical 3.5 MeV alpha particle orbit undergoing TF ripple diffusion and ultimately lost to the alpha particle detector for the baseline $I = 1.4$ MA case. This orbit had a pitch angle of $\chi = 69°$ and was launched 'backwards in time' from an aperture location of $r_{\rm ap} = -2$ cm. The banana tips were in a relatively high ripple region, and so their vertical displacements due to SRD were relatively large.

of the magnetic axis and (circular) plasma boundary, the shape of the plasma pressure profile, the toroidal magnetic field at the magnetic axis and a model for the vacuum magnetic fields (outside the plasma but inside the limiter shadow).

A single SRD loss orbit calculated for the baseline $I = 1.4$ MA case using this code is shown in Fig. 3. For this case the banana tip was started in a relatively high ripple region where successive poloidal transits had a large random vertical displacement. The numerical accuracy of this code is such that when the TF ripple and collisionality are set to zero, orbits such as that in Fig. 3 can circulate for more than 50 000 transits without any significant radial motion due to numerical error (<0.1 cm).

Another important factor in the TF ripple loss modelling is Coulomb collisions, which cause alpha particle banana orbits to change their magnetic moment and/or move from confined to unconfined regions. Previous numerical modelling of TFTR has shown that collisions can increase the total alpha particle ripple loss by about a factor of 2 [21, 22]. The main factor determining the collisional effect is the ratio of the alpha particle pitch angle scattering frequency $\nu_{\alpha,\perp}$ (i.e. the e-folding rate of $v_\perp^2$) to the alpha particle energy e-folding rate $\nu_{\alpha,E}$, which is [24]

$$\nu_{\alpha,\perp}/\nu_{\alpha,E} \approx 100 Z_{\rm eff}(T_{\rm e}/E_\alpha)^{3/2}. \quad (3)$$

At the plasma axis, this ratio is ≈1/50 for 3.5 MeV alpha particles with $T_{\rm e}(0) = 5.5$ keV and $Z_{\rm eff} = 3$

(Table I). However, since in this code these collision times are assumed to be constant versus radius, this ratio is taken to be characteristic of conditions near the SRD boundary ($n_e = 2.7 \times 10^{13}$ cm^{-3} and $T_e \approx 3.5$ keV), i.e. $\tau_{\alpha,E} = 1/\nu_{\alpha,E} \approx 0.1$ s and $\tau_{\alpha,\perp} = 1/\nu_{\alpha,\perp} \approx 0.10$ s for all cases.

The modelling of alpha particle ripple loss for this experiment was done using a Monte Carlo technique similar to that described in Refs [21, 22], in which 3.5 MeV alpha particles are started at random pitch and toroidal angles with a radial distribution fit to the measured alpha particle source profiles. The alpha particle birth profiles in this experiment were very centrally peaked, with about 80% of the alpha particle banana tips born on initially confined orbits. For each plasma type, the ORBIT code run was started with a total of 1000 alpha particles born at 3.5 MeV, which were distributed to match the measured alpha particle source profile versus radius and randomly in pitch angle and toroidal angle. Each particle was followed for 75 000 toroidal transits (about one energy e-folding), or until the particle hit the wall. The number of alpha particles was limited by the available time on the VAX Alpha computers at PPPL (each run took about 2 to 3 weeks).

Maps of the calculated alpha particle loss regions versus R and χ for the baseline case are shown in Ref. [17]. Roughly speaking, all alpha particle orbits with banana tips outside a circle of radius 25 cm centred at $R = 2.6$ m and $z = 0$ are lost either owing to collisional ripple diffusion or first orbit loss, the latter being localized outside a circle of radius 40 cm centred at $R = 2.75$ m and $z = 0$. For orbits born along the outer midplane, the collisional ripple diffusion occurs mainly for orbits near the co-side of the passing–trapped boundary.

Results from the Monte Carlo modelling for the baseline $I = 1.4$ MA case are shown in Fig. 4. Most of the ripple-lost alpha particles hit the first wall at poloidal angles between 0 and 30° below the outer limiter and at pitch angles near $\chi = 60°$, as expected from previous calculations [11–13, 21, 22]. The alpha particle energy loss spectrum has a spike at the birth energy due to first orbit loss (not shown) and a low energy tail due to collisional ripple loss. The total TF ripple loss fraction was ≈7% for this case, while the total first orbit loss fraction was ≈15%. Further results of the TF ripple modelling are discussed along with the experimental data in Section 5.

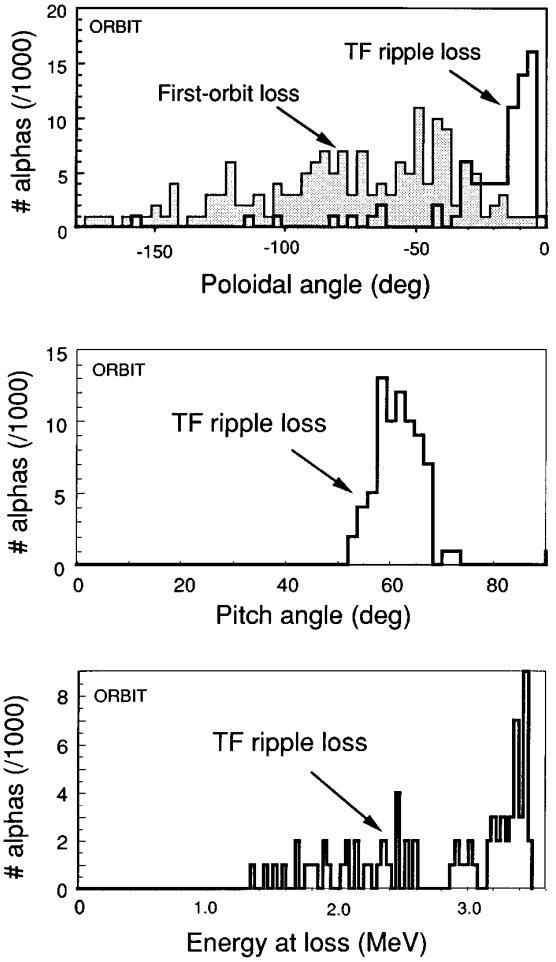

FIG. 4. Results from the Monte Carlo ORBIT code modelling of the baseline case using 1000 alpha particles followed for one energy e-folding time. The ripple loss is concentrated within a poloidal angle of ≈ 30° below the outer midplane. The middle frame shows that the pitch angle distribution of ripple loss is peaked at $\chi \approx 60°$ with respect to the total magnetic field. In the bottom frame the energy spectrum is shown of the alpha particle ripple loss, which has an average energy of ≈2.5 to 3.0 MeV, owing to delayed collisional loss (the first orbit loss at 3.5 MeV is not shown). These results are similar to previous modelling of TFTR ripple loss and are insensitive to the choice of vacuum fields.

5. EXPERIMENTAL RESULTS AND COMPARISON WITH ORBIT MODELLING

This section contains a comparison of the midplane lost alpha particle measurements with the numerical results from the ORBIT guiding centre model for

alpha particle ripple loss. Sections 5.1, 5.2 and 5.3 describe, respectively, the measurements and modelling of the total alpha particle loss, pitch angle and perpendicular gyroradius distributions. A summary of some additional observations is presented in Section 5.4.

The strategy of this analysis is to compare the experimental results with the ORBIT code modelling and to show where this modelling is successful and where it is not. The main deficiency of this model is an inability to explain the radial profile of the data, which leads to a discussion of the limiter shadowing effect in Section 6.

5.1. Neutron normalized alpha particle loss

There were a total of 34 DT discharges for the three plasma scans in this experiment: (a) the '$q(r)$ scan', (b) the '$q(a)$ scan' and (c) the 'ρ scan' (Section 2). For each type of discharge within these scans, alpha particle loss data were taken for three different midplane detector aperture positions, namely, $r_{ap} = -2.0$ cm, -0.5 cm and $+1.0$ cm with respect to the geometrical shadow of the outer limiter. One baseline case was common to each of these scans ($I = 1.4$ MA, $B = 4.7$ T). A detailed list of discharges and some examples of the raw data are in Ref. [17].

The total alpha particle loss is defined as the total scintillator light collected by this detector integrated over its χ and ρ acceptance range, after subtracting the background fluorescence of the fibreoptic bundle [17, 25]. Unless otherwise noted, the alpha particle loss will be averaged over the quasi-steady-state period from 4.5 to 4.8 s near the end of neutral beam injection (NBI) (Fig. 1). The neutron normalized alpha particle loss is defined as the total alpha particle loss divided by the DT neutron rate, averaged over the same time period.

The alpha particle collection fraction, i.e. the absolute value of the neutron normalized alpha particle loss into this detector, was estimated by cross-calibrating the midplane alpha particle loss with the detector at the bottom of the vessel. The alpha particle loss to the bottom detector was assumed to be due to first orbit loss, as has been found previously for very similar DT discharges [14], and the alpha particle energy of the midplane probe signals was assumed to be 3.5 MeV for this estimate.

The resulting midplane alpha particle collection fraction versus the detector aperture position for the baseline plasma case is shown in Fig. 5. The inferred

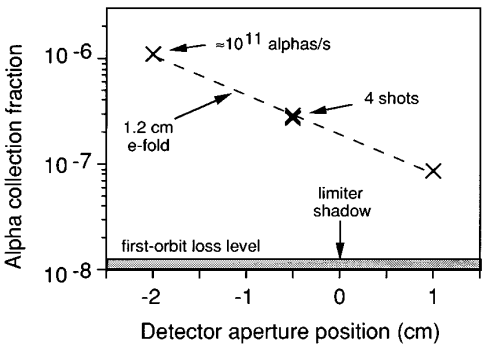

FIG. 5. Alpha particle collection fraction, i.e. the alpha particle flux measured by the midplane detector divided by the global DT neutron rate, as a function of the aperture position for the baseline case. The absolute value of the alpha particle loss was obtained by comparing the midplane signals with the bottom detector signals, assuming that the latter were due to first orbit loss [14]. The alpha particle collection fractions were much larger than the first orbit loss calculated for the midplane detector, and decreased with an e-folding length of ≈1 to 2 cm over the range of aperture positions used in this experiment.

alpha collection fraction was in the range $F \approx 10^{-6}$ for the $r_{ap} = -2.0$ cm position to $F \approx 10^{-7}$ for the $r_{ap} = +1.0$ cm position, i.e. the alpha particle flux into the detector was $\approx 10^{10}$ to 10^{11} alpha particles/s at the typical neutron rate of $\approx 10^{17}$ n/s in this experiment. This alpha particle collection fraction was ≈10 to 100 times larger than the expected first orbit loss collection fraction for this detector, as calculated using the same Lorentz orbit code used for the bottom detector [14]. Thus, the first orbit loss contribution to the midplane alpha particle loss signals was negligible for the range of aperture positions used in this experiment. Note that the first orbit loss of DD fusion products identified previously at the midplane was seen only for aperture positions $r_{ap} \approx +10$ cm [11, 12] where the TF ripple loss was much smaller (Section 6).

The relative variation of the neutron normalized alpha particle loss for the three plasma scans in this experiment is shown in Fig. 6 as a function of the scanning variable. All the alpha particle loss data in Fig. 6 are normalized such that the alpha particle loss was unity for the baseline case at the middle aperture position ($r_{ap} = -0.5$ cm). The same data are shown in another way in Fig. 7, along with the TF ripple loss calculated from the ORBIT code for each plasma type. For each aperture position in Fig. 7, the alpha

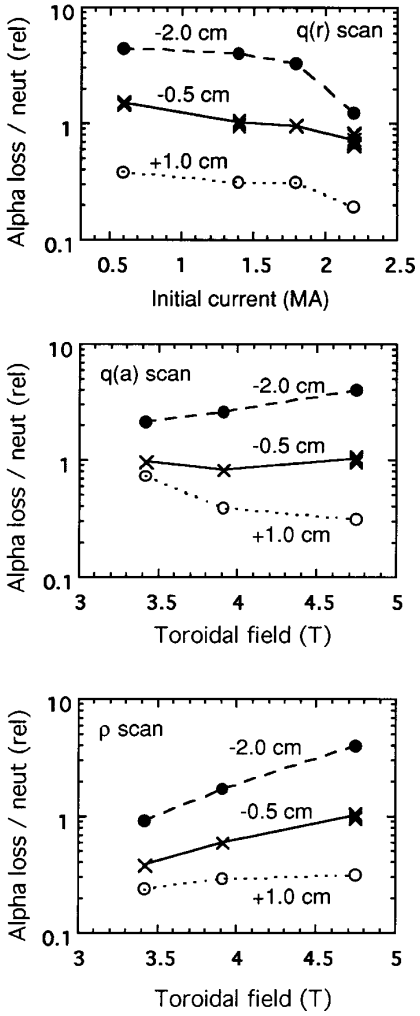

FIG. 6. Variations of the midplane alpha particle loss for the various plasma scans and aperture positions. All the data are normalized such that the baseline case at $r_{ap} = -0.5$ cm is unity. Two general trends are for the alpha particle loss to decrease with a more peaked current profile, i.e. high central $q(r)$, and for the alpha particle loss to decrease with decreasing B at constant $q(a)$. All the data are averaged over the steady state period from 4.5 to 4.8 s during NBI.

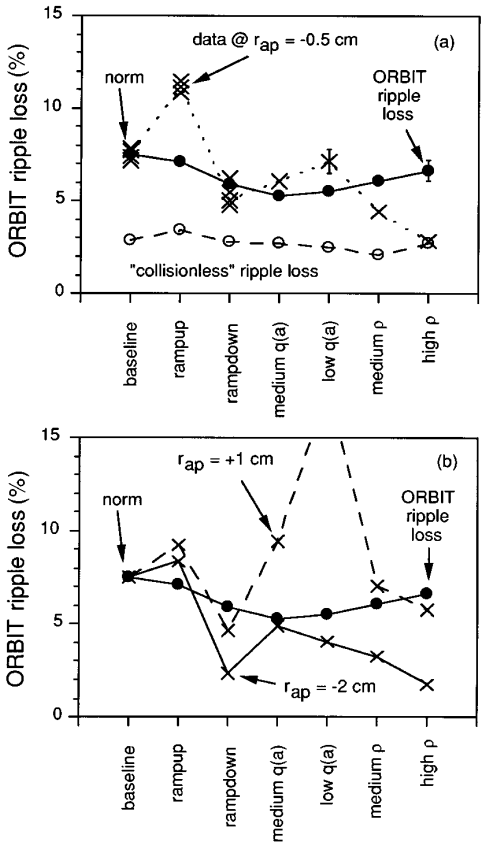

FIG. 7. Neutron normalized midplane alpha particle loss for the various plasma scans, compared with the total TF ripple loss of alpha particles as calculated by the ORBIT guiding centre code (the data points are the same as for Fig. 6). The data are normalized to the baseline ORBIT calculation for each probe position, and the lines are solely to guide the eye. The measured alpha particle loss varies by a factor of 3 for the $r_{ap} = -0.5$ cm case, and somewhat more (less) for the $r_{ap} = -2.0$ cm (+1.0 cm) cases (the off-scale point may have been affected by a locked mode). There is no clear correlation between the measured variations and the calculated ORBIT code results, either for the full collisional slowing down time (closed circles) or for the 'collisionless' result evaluated after only 5000 transits.

particle loss in the baseline case was normalized to the total ripple loss calculated by ORBIT, so that the relative variations for the different types of $q(r)$ profiles can be seen. The shot-to-shot variability of the neutron normalized alpha particle loss for a given plasma type and aperture position was only ≈5%, and the estimated systematic uncertainty was about ±10 to 20% from type-to-type.

Looking first at the data and modelling the results for the middle $r_{ap} = -0.5$ cm cases, the following trends were seen with respect to the baseline:

(a) *For the $q(r)$ scan* the measured alpha particle loss increased by ≈50% for the current rampup case and decreased by ≈30% for the current rampdown case, whereas the calculated global ORBIT ripple loss decreased by ≈6% and 17%, respectively.

(b) *For the $q(a)$ scan* the measured alpha particle loss decreased by ≈20% and 5% for the medium and low $q(a)$ cases, respectively, whereas the calculated ORBIT results decreased by ≈30% and 25%, respectively.

(c) *For the ρ scan* the measured alpha particle loss decreased by ≈40% and 60% for the medium- and low-B cases, respectively, whereas the calculated ORBIT results decreased by ≈20% and 10%, respectively.

The qualitative trends at the other aperture positions were fairly similar, except for the low-$q(a)$ case at $r_{ap} = +1.0$ cm, which may have been affected by a stationary magnetic perturbation (Section 5.4).

In general, the trends in the alpha particle loss data are not well explained by the ORBIT modelling. The variation in the measured alpha particle loss at a given aperture position was up to a factor of ≈4 between different plasma types, but the range in the ORBIT calculated global ripple loss was only ≈5% to 8%, i.e. a variation of less than a factor of 2. In addition, the highest measured loss (i.e. the current rampup cases) did not correspond to the highest calculated loss, and the lowest measured loss (i.e. the low-B constant $q(a)$ case) did not correspond to the lowest calculated loss.

It is highly unlikely that these large differences between experiment and modelling can be attributed to statistical uncertainties in the calculated alpha particle ripple loss fractions. These uncertainties were estimated by dividing each 1000 particle run into ten 100 particle sub-samples, and finding the standard deviation of the resulting ten alpha particle loss fractions from their mean, which was only about ±0.5% (i.e. the average result was ≈7.5 ± 0.5% for the baseline case). The sensitivity of the global ripple loss to various modelling assumptions is illustrated in Table II. For example, a variation in the assumed alpha particle source profile $S_\alpha(r) = [1 - (r/a)^2]^{S_{exp}}$ from $S_{exp} = 6.7$ to 5.7 (about the expected experimental uncertainty) caused an insignificant change in the 'collisionless' ripple loss after only 5000 transits. The ratio of the 'collisional' (i.e. with 50 000 transits) to the collisionless results was ≈2 to 2.5 in all cases, as shown in Fig. 7(a).

The conclusion from this analysis is that the measured variations in the total alpha particle loss in these $q(r)$ and ρ scans were not well explained by the ORBIT ripple loss calculations. Furthermore, the strong dependence of the measured alpha particle signals on the radial aperture position could not be predicted from the ORBIT code model, which assumed a smooth toroidal first wall. Although the absolute magnitude of the alpha particle loss to this midplane detector was much larger than the first orbit loss, as expected from Fig. 4, the absolute level of alpha particle loss was not explained by this ORBIT modelling. Further analysis of these data requires a supplementary limiter shadowing model, as described in Section 6.

Table II. Sensitivity of ORBIT Calculations (Baseline Case)

	Loss after 5000 transits (%)	Loss after 50 000 transits (%)
Standard model[a]	2.9	6.7
Standard model with lower δE[b]	2.7	5.4
Improved vacuum (1000)[c]	3.0	7.1
Improved vacuum (2500)[d]	3.2	6.6
Broader source profile[e]	2.9	—
No ripple with collisions[f]	1.2	—
No ripple, no collisions[g]	0.2	—
Larger ripple with collisions[h]	7.9	—

[a] Standard model results shown with outer limiter $q = 10$ and a shift of −5 cm.
[b] Numerical accuracy increased from $\delta E = 5 \times 10^{-8}$ to 5×10^{-9} per step.
[c] Standard model but with outer limiter $q = 25$ and a shift of −17 cm (1000 alpha particles).
[d] Same as (c) but with 2500 alpha particles.
[e] Alpha particles source broadened from $S_{exp} = 6.7$ to $S_{exp} = 5.7$, where $S_\alpha(r) = [1 - (r/a)^2]^{S_{exp}}$.
[f] Ripple turned off, collisions retained.
[g] Ripple and collisions turned off.
[h] Standard case with three times the normal ripple level.

5.2. Pitch angle variations

The pitch angle of the alpha particle loss is important to help identify the loss mechanism, since the SRD induced loss is expected only in a relatively narrow range of pitch angles. The experimental pitch angles are measured with respect to the toroidal magnetic field at the detector, which is only ≈1° less than the pitch angle with respect to the total magnetic field due to the large $q(a_{lim}) \approx 25$ near the outer limiter (Appendix). All the distributions discussed below are averaged over the perpendicular gyroradius range $\rho = 2$–12 cm and over the time of 4.5 to 4.8 s.

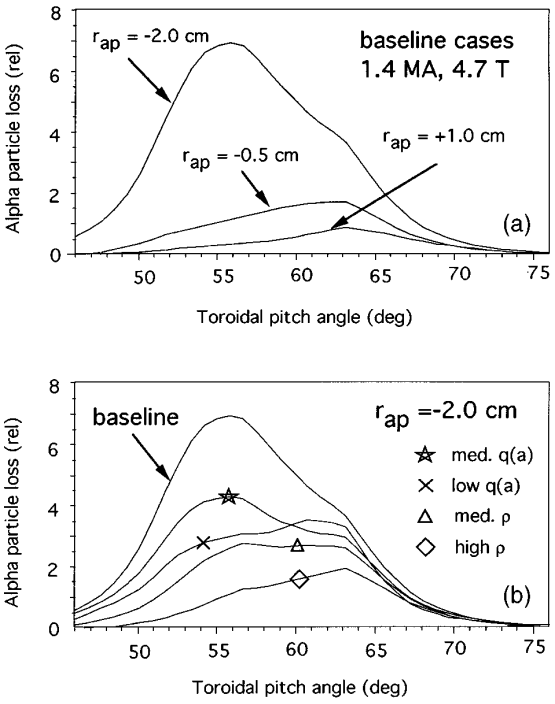

FIG. 8. Examples of pitch angle distributions of the midplane alpha particle loss measured in this experiment: (a) variation with aperture position for the baseline case, (b) variation with plasma type for $r_{ap} = -2.0$ cm (the relative amplitudes for each signal are also shown). These pitch angles are measured with respect to the total magnetic field at the detector and have a systematic uncertainty of about $\pm 3°$.

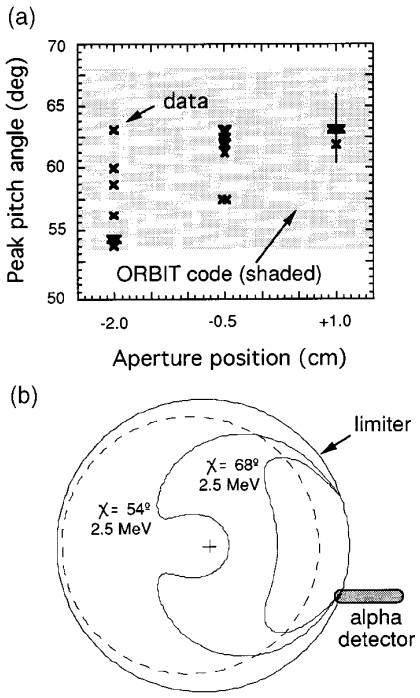

FIG. 9. (a) Comparison between the peak pitch angles in the data and the expected range of pitch angles for TF ripple loss based on the ORBIT code. The data all fall within the expected range, but the model does not predict the systematic variation of the measured pitch angles versus the aperture radius. All the data are averaged over the steady state period from 4.5 to 4.8 s during NBI. (b) Examples of two $E = 2.5$ MeV alpha particle orbits entering the detector for the extremes of this pitch angle range for the baseline case.

Figure 8 shows the variation in the shapes of the measured pitch angle distributions versus the detector aperture position for the baseline case (Fig. 8(a)) and for different $q(r)$ cases at $r_{ap} = -2.0$ cm (Fig. 8(b)). In general, these distributions seem to consist of two distinct components: one near $\chi \approx 64°$ (particularly dominant at the larger aperture radii), and another at $\chi \approx 54°$ (particularly dominant at the smaller aperture radii). The instrumental resolution of $\approx 6°$ FWHM limits the ability to distinguish between these two components, and there is a potential systematic alignment uncertainty of $\pm 3°$.

The pitch angle distribution calculated for SRD by the ORBIT code was shown in Fig. 4 for the baseline case. The other six cases showed the same result to within the statistical uncertainties; namely, that the alpha particle loss due to SRD was localized within the pitch angle range $\chi \approx 54$–$68°$. The measured peaks of the pitch angle distributions versus aperture radius are shown in Fig. 9(a), along with the range of the pitch angles predicted for TF ripple loss by the ORBIT code. All the data fall within the expected range for SRD corresponding to trapped alpha particle orbits, as illustrated in Fig. 9(b). However, the code does not explain the systematic variation of the data with the aperture radius, and the statistical uncertainties in the code results are too large to explain the differences among the pitch angle distributions for the various examples in Fig. 8. The conclusion from this comparison is that the measured pitch angle distributions are consistent with TF ripple loss, but that their variations with $q(r)$ cannot be explained by the ORBIT code. Further analysis of these data using a supplementary limiter shadowing model is described in Section 6.

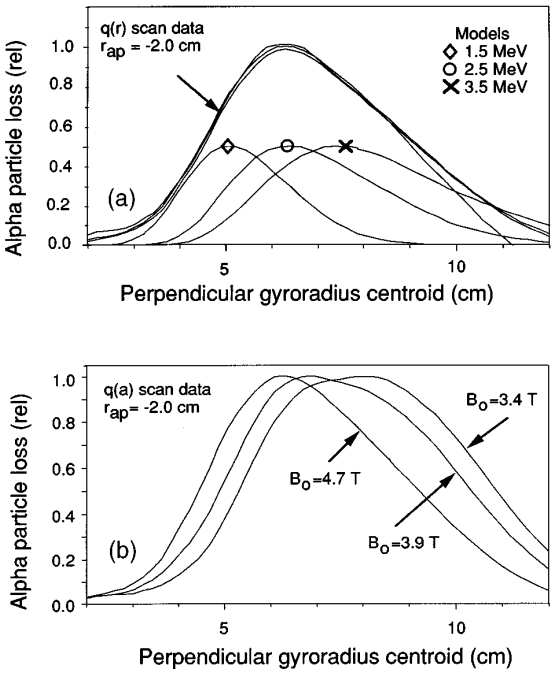

FIG. 10. Examples of the perpendicular gyroradius distributions of the midplane alpha particle loss measured in this experiment. (a) The three plasmas in the $q(r)$ scan at $B_0 = 4.7$ T (normalized to each other vertically), along with model distributions for various assumed alpha particle energies. (b) The three plasmas for the $q(a)$ scan in which B_0 was varied, showing an increase in the alpha particle perpendicular gyroradius due to the decreasing B.

5.3. Perpendicular gyroradius (energy) variations

The alpha particle perpendicular gyroradius distributions can in principle be used to determine the energy spectrum of the alpha particle loss, which can be compared with the predictions from the ORBIT code (Fig. 4). However, the design of the detectors was optimized for pitch angle and not for perpendicular gyroradius resolution, so only the average energy of the alpha particle loss can be determined and not its energy distribution function.

Examples of the measured alpha particle perpendicular gyroradius distributions for this experiment are shown in Fig. 10, where in each case the data were averaged over the pitch angle range $\chi = 45$–$75°$ between 4.5 and 4.8 s. The distributions for the three shots in the $q(r)$ scan, all for the same aperture position of $r_{ap} = -2.0$ cm and $B_0 = 4.7$ T, are shown in Fig. 10(a). The measured distributions for the three

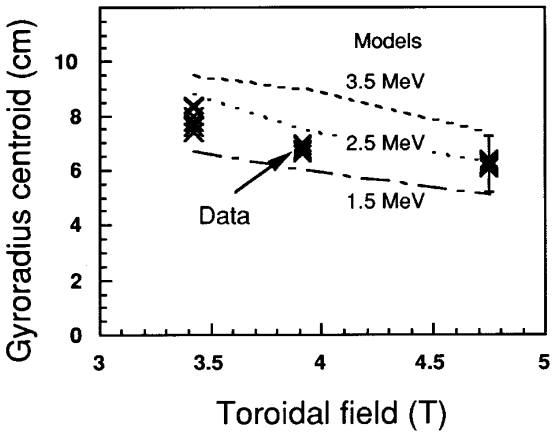

FIG. 11. Comparison between the peak of the measured perpendicular gyroradius distributions with the peak locations expected for alpha particle loss of various energies. At full toroidal field all cases have very nearly the same peak perpendicular gyroradius, which by comparison with the models implies a mean alpha particle loss energy of $E = 2.5 \pm 1$ MeV. At lower fields the inferred average energy appears to be somewhat lower, but the uncertainties are also larger. All data are averaged over the steady state period from 4.5 to 4.8 s during NBI.

shots in the $q(a)$ scan, again for $r_{ap} = -2.0$ cm, are shown in Fig. 10(b). There is a relatively large instrumental spread of the data in the perpendicular gyroradius centroid co-ordinate direction due to the finite size of the detector apertures; thus the average alpha particle perpendicular gyroradius can only be estimated by comparing the data with modelled distributions based on the detector aperture and scintillator geometry, some of which are also shown in Fig. 10(a).

The three shots of the $q(r)$ scan in Fig. 10(a) have the same perpendicular gyroradius distribution shapes, implying that the energy spectrum of the alpha particle loss was not sensitive to this $q(r)$ variation. The best fit is for $E = 2.5$ MeV, but the systematic uncertainty in the perpendicular gyroradius centroid co-ordinate is about ± 1 cm, so the results at full field are consistent with the alpha particle loss at $E = 2.5 \pm 1$ MeV. The three shots of the $q(a)$ scan in Fig. 10(b) show an increase in the gyroradii with decreasing B, but this is mainly due to the change in B itself.

The peak gyroradii centroids during the steady state period from 4.5 to 4.8 s for all plasmas in this experiment are shown in Fig. 11 as a function of B, along with model calculations for various energies. The inferred average alpha particle loss energy

is $E \approx 2 \pm 1$ MeV for the $B_0 = 3.9$ T and 3.4 T cases. However, the instrumental uncertainties for larger gyroradii are higher [17], so the fact that the inferred alpha particle loss energy is lower in the case of $B_0 = 3.4$ T than it is in the case of $B_0 = 4.7$ T may not be significant.

The strongest conclusion from this analysis is that the average energy of the alpha particle loss is insensitive to both the type of plasma and the aperture position in this experiment. This is also the result of the modelling of collisional ripple loss for these cases, to within the statistical uncertainties (e.g., Fig. 4). However, the relatively poor energy resolution and systematic uncertainties in this measurement prevent a more quantitative comparison with the ORBIT results.

5.4. Additional observations

The typical time dependence of the midplane alpha particle loss signal with respect to the neutron signal (i.e. alpha particle source rate) was shown in Fig. 1. For almost all plasmas and aperture positions, the relative alpha particle loss per neutron was constant (to within about ±20%) during the time interval between ≈50 ms after the start of NBI and 200 ms after the end of NBI, similar to the behaviour observed previously for an $I = 2.0$ MA case [13].

The expected time dependence for collisional TF ripple loss can be estimated from the energy spectrum of ripple loss calculated by the ORBIT code (Fig. 4). For all cases, about two thirds of the collisional TF ripple loss occurred within ≈30 ms of the alpha particle birth, i.e. within about a third of an energy slowing down time. This is very fast with respect to the ≈250 ms risetime of the alpha particle source rate during NBI (Fig. 1), and so is consistent with the constant alpha particle loss per neutron observed during NBI. After NBI ends the global alpha particle source rate e-folds in only ≈75 ms, so an increase in the alpha particle loss per neutron of ≈60% is expected ≥0.1 s after the end of NBI. This increase is larger than the ≤20% increase observed in the data. However, interpretation of this difference requires a time dependent analysis of the ripple loss, including evolution of the equilibrium, source profile and collisionality after the end of NBI, which is not possible with the present ORBIT code.

Some of the discharges in this experiment had relatively large sawteeth during NBI, which are common in TFTR at low NBI power and low $q(a)$. However, in all these cases the alpha particle loss per neutron was constant except for a very brief (≈100 μs) increase in alpha particle loss by a factor ≤3 just at the sawtooth crash, similar to that seen previously for DD fusion products [26]. This burst had a negligible effect on the alpha particle loss averaged over 4.5 to 4.8 s, and so does not affect the interpretation of the signals of Section 5.1, part (c). The only other visible MHD effect was an ≈20% effect of stationary magnetic perturbations (SMPs) on the alpha particle loss signals. These SMPs (sometimes called 'locked modes') are measured on TFTR by a pair of radial field coils [27], and occurred for many of the current rampdown discharges in this experiment. Such MHD effects on the alpha particle loss cannot be understood without a set of ORBIT calculations that include these low-n magnetic perturbations, which is beyond the scope of this article.

A separate radial probe scan was made in $R_0 = 2.45$ m plasmas with the same plasma current and toroidal field as the baseline $R_0 = 2.52$ m plasma discussed above (i.e. $I = 1.4$ MA, $B_0 = 4.7$ T). These smaller major radius plasmas allowed a larger inward scan of the probe aperture to $r_{ap} = -6.5$ cm, since the plasma edge was further from the outer limiter at the probe. The level of the normalized alpha particle loss per neutron for the $r_{ap} = -0.5$ cm position was the same as for the baseline $R_0 = 2.52$ m plasmas within ±5%, but the signal at $r_{ap} = -2.0$ cm for the $R_0 = 2.45$ m plasma was a factor of ≈2 lower than that for the $R_0 = 2.52$ m plasma. As the detector was moved further inward for the $R_0 = 2.45$ m case, the loss saturated at $r_{ap} = -5$ cm at 4 times the level of that at $r_{ap} = -2.0$ cm. In general, these results (as well as the pitch angle and perpendicular gyroradius distributions) were qualitatively similar to those for the $R_0 = 2.52$ m plasmas above [17].

Near the end of the TFTR DT run another midplane probe scan at $R_0 = 2.52$ m was made to obtain a more complete radial profile (these data were taken about 1.5 years after those in Sections 5.1 to 5.3). In this extended scan the aperture was moved inward by an additional 4.5 cm to $r_{ap} = -6.5$ cm in plasmas essentially the same as those in the baseline case described above. Although the results described in Sections 5.1 to 5.3 were highly reproducible during the period in which they were taken, the results of this extended probe scan were considerably different [17]. For example, at $r_{ap} = -2$ cm the total alpha particle flux (per neutron) was ≈4 times smaller and had a different pitch angle distribution for the later scan, and the radial e-folding length within the region of overlap was longer by a factor of ≈3. This

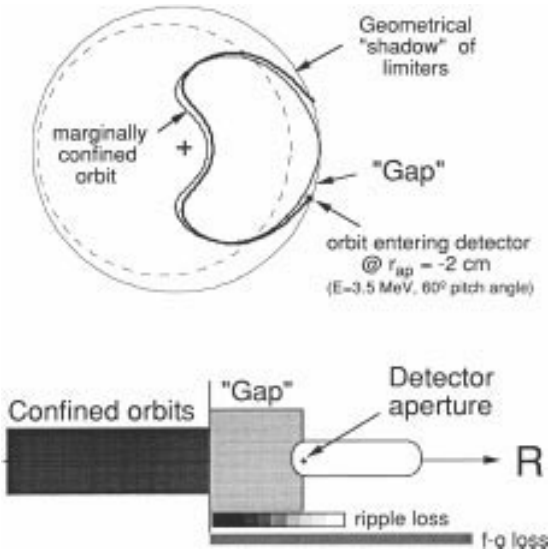

FIG. 12. Illustration of the limiter shadowing effect for alpha particle orbits entering the detector aperture near the outer midplane. In the absence of SRD, an alpha particle launched backwards in time from the detector intersects the geometrical shadow of the limiter near the outer midplane within one poloidal transit. The marginally confined orbit of the same energy and pitch angle is separated from the detector aperture by a radial 'gap' over which alpha particles must jump in order to be detected. The expected radial profile of SRD induced loss and first orbit loss is shown schematically at the bottom.

unexpected difference was possibly due to the installation of an IBW antenna, which was added just before the extended scan. The specific cause of this difference is not understood, since there is insufficient information concerning the RF antenna location; however, it is very likely that the quantitative details of the midplane alpha particle loss signals versus aperture position are very sensitive to the limiter structure, as discussed further in Section 6.

6. LIMITER SHADOWING EFFECTS

The attempts made in Section 5 to understand the midplane alpha particle loss measurements in terms of the global ORBIT code ripple loss modelling were not very successful. The clearest problem was that this model could not explain the strong radial dependence of the total alpha particle loss illustrated in Fig. 6, since the code assumed that all the alpha particles are lost to a smooth toroidal wall at the geometrical shadow of the limiters.

The purpose of this section is to clarify how the actual highly non-smooth limiter geometry can affect the interpretation of the local detector signals. This occurs when the escaping alpha particle orbits hit the outer limiters before they reach the detector aperture. In this section the results of the ORBIT code are supplemented by some modelling of this limiter shadowing effect, but these modifications are not yet accurate or complete enough to quantitatively explain the experimental data. Possible improvements in the modelling are discussed in Section 7.

6.1. Orbit gaps and jumps near the outer midplane

The basic geometry of the limiter shadowing effect in TFTR is shown in Fig. 12. Without any TF ripple in the guiding centre ORBIT calculation, a 3.5 MeV alpha particle orbit which is launched backward in time from the detector aperture at $r_{\rm ap} = -2.0$ cm hits the geometrical shadow of the limiter near the outer midplane before completing one poloidal transit. Since there are several outer midplane limiters in TFTR (Section 3), and since $q(r) \approx 20$–30 near the outer limiter (Appendix), these limiters can shadow nearly all the alpha particle orbits before they can enter the detector aperture.

Therefore, there is a minimum radial 'gap' over which a confined alpha particle orbit must 'jump' before it can reach the detector aperture, even when the aperture is slightly inside the geometrical shadow of the limiter. This gap Δ_r is determined by the aperture location and by the shape of the outer limb of the marginally confined alpha particle orbit, as illustrated in Fig. 12. If the radial jumps δ_r are diffusive, and if the aperture is within the gap (i.e. $\Delta_r > 0$), then the detected ripple loss signal should decrease with increasing $r_{\rm ap}$, in qualitative agreement with the data. In contrast, the expected profile for first orbit loss should be nearly flat in this region since the radial jumps are not diffusive but occur in a single large step.

Figure 13 illustrates calculations of typical radial gaps for an aperture position of $r_{\rm ap} = 0$ cm as a function of the alpha particle pitch angle and energy. The marginally confined orbits all intersect the limiter at the outer midplane over this range of energy and pitch angle. These gaps were calculated numerically using the ORBIT code for the baseline case using a model for the q and Shafranov shift at the outer limiter (Appendix). For example, alpha particles with $E = 2.5$ MeV and $\chi \approx 60°$ have a gap of

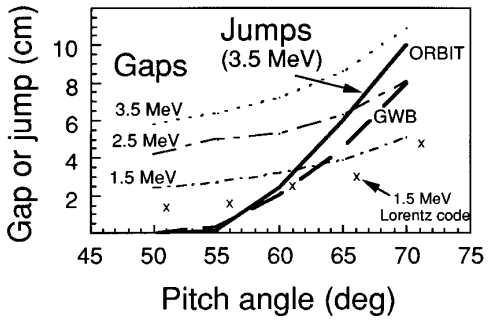

FIG. 13. Calculated radial 'gaps' between the marginally confined alpha particle orbits and the geometrical shadow of the outer limiter at the detector location, as a function of the alpha particle energy and pitch angle. The gaps are smaller for lower energy and lower pitch angle alpha particles since the shifts of the orbit from the flux surfaces are smaller. The average radial 'jumps' per transit due to stochastic TF ripple diffusion are also shown, both from numerical calculations using the ORBIT code and from Eq. (1). The gaps for $E = 1.5$ MeV calculated using a more accurate vacuum model in the finite perpendicular gyroradius orbit code are also shown for comparison.

$\Delta_r \approx 5$ cm, i.e. in the absence of radial diffusion, the alpha particle orbits will intersect the limiter before entering the aperture only for $r_{\rm ap} \geq -5$ cm. For lower energy and lower pitch angle alpha particles the gaps tend to be smaller, since the shifts of their banana orbits from the flux surfaces are smaller.

Also shown in Fig. 13 are more accurate calculations of the gaps for the $E = 1.5$ MeV case made using a Lorentz orbit code which includes a full 2-D model of the magnetic flux surfaces. The gaps are ≈1 cm smaller than for the approximate ORBIT calculations and become less than $\Delta_r \approx 2$ cm for pitch angles below $\chi \approx 60°$. The actual gaps are further reduced by the ≈0.6 cm radial wobble of the total magnetic field due to the TF ripple near the outer midplane, which was not present in either calculation. Therefore, alpha particles with low enough energy ($E < 2$ MeV) and pitch angle ($\chi < 60°$) can become unshadowed by the limiter at $r_{\rm ap} = -2$ cm, depending on the exact vacuum fields. This is important since then the detector can collect a different class of 'confined' alpha particles (Section 6.3).

The extent to which alpha particles can cross this gap on their last poloidal transit depends on their radial 'jumps' due to SRD. These jumps occur at the banana tips with a vertical displacement of approximately [1]

$$\delta_{\rm v} \approx (N\pi/\sin\theta)^{1/2}(q/\varepsilon)^{3/2}\ \rho\delta\sin(N\phi) \qquad (4)$$

where θ and ϕ are the poloidal and toroidal angles of the banana tip (see under Eq. (1) for other definitions). The physical cause of these jumps is the change in the alpha particle drift motion caused by the ripple in the magnitude of B near the banana tips. These jumps are oscillatory for small ripple, but become random when the particle 'islands' in banana tip phase space (e.g. r, θ) begin to overlap [1, 2, 17]. For most alpha particles entering the detector the SRD threshold criterion (Eq. (1)) is satisfied and these jumps are effectively random on successive banana tips.

Typical magnitudes of these SRD induced jumps for 3.5 MeV alpha particles are also shown in Fig. 13, both from a numerical calculation using the ORBIT code and from the analytic formula given by Eq. (4). Note that the radial jumps as measured at the outer midplane are 2 to 3 times larger than the corresponding vertical jumps at the banana tip, owing to the shape of the banana orbit. These jumps are typically $\delta_r \approx 3$ cm for $E = 2.5$ MeV and $\chi \approx 60°$, i.e. comparable to the radial gaps. For a given alpha particle energy, the jumps increase rapidly with pitch angle as the banana tip location falls in a higher ripple region. There are two such jumps between the marginally confined orbit and the detector aperture. Thus, there is a significant probability that alpha particles undergoing SRD can jump over the gaps and enter the detector aperture.

6.2. Probability of missing the limiter

The ORBIT code with the TF ripple present was used to estimate the probability that SRD allowed the alpha particles to jump these gaps. Alpha particles were launched at the detector aperture and allowed to move 'backwards in time' into the plasma, and the fraction of alpha particles that missed the limiter after their first poloidal transit was taken as being proportional to the probability of alpha particles reaching the detector from the plasma. An example of such an alpha particle orbit was shown in Fig. 3. For alpha particles of a given energy and aperture location, 1000 alpha particle orbits were launched at each pitch angle with varying toroidal angles to simulate the alpha particles which are actually diffusing outward because of TF ripple diffusion after many confined transits.

The results of this simulation for the baseline case are shown in Fig. 14. For the aperture position $r_{\rm ap} = -0.5$ cm (Fig. 14(a)), the probability of missing the limiter on the first poloidal transit is found to

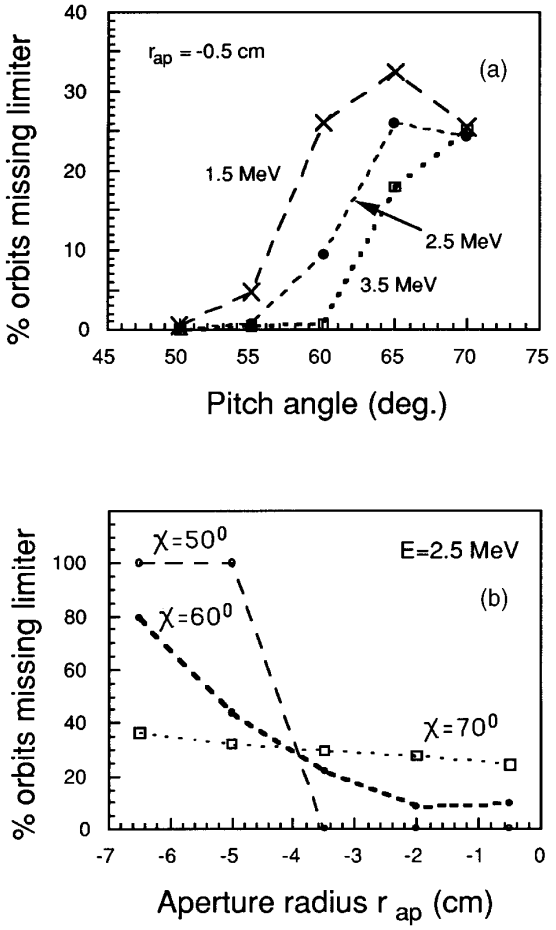

FIG. 14. Plot of the calculated probability that an alpha particle orbit launched from the detector aperture misses the outer limiter on its first poloidal transit. (a) This probability increases with pitch angle, since the jumps are larger for orbits with banana tips in a higher ripple region (Fig. 13). (b) The probability of missing the limiter increases as the aperture is moved inward to narrow the gap. For alpha particles with low pitch angles, this increase occurs only when the gap is nearly zero, since the diffusive jump size is very small for banana tips near the stochastic threshold.

increase with increasing pitch angle, as expected from the larger jumps at higher pitch shown in Fig. 13. At pitch angles χ between 55 and 65° the probability of missing the limiter also increases with decreasing energy at a given pitch angle, since the gaps are smaller (the jumps decrease linearly with perpendicular gyroradius according to Eq. (4), but the banana tip locations move to larger ripple as the energy is reduced for a given pitch angle).

For a typical energy of $E = 2.5$ MeV, the probability of missing the limiter on one poloidal transit also varies with the assumed aperture position, as shown in Fig. 14(b). At $\chi = 50°$ the probability increases sharply from nearly 0 to 1 at the edge of the gap, since the jumps are very small or zero for these orbits near the SRD boundary. At $\chi = 60°$ the probability starts to increase only for $r_{ap} < -2$ cm, while for $\chi = 70°$ the probability is approximately independent of r_{ap} since the jumps are so large. Thus, the limiter shadowing probability calculated in this way is a sensitive function of aperture position, energy and pitch angle.

These results are qualitatively similar to previous calculations of the limiter shadowing effect done to simulate the midplane probe signals in both DD [12] and DT discharges [20]. However, in Ref. [12] the magnetic geometry was highly simplified (e.g., no Shafranov shifts), so the gaps were not calculated accurately, and in Ref. [20] the limiter shadowing probability per poloidal transit was approximated by a single probability independent of energy and pitch angle. However, the present probability model is also incomplete and quantitatively inaccurate since it evaluates the limiter intersection only on the first poloidal transit, and does not attempt to calculate the history of the alpha particle orbit all the way back to its birth, owing to limitations in the computing time available (Section 7.2).

6.3. Comparisons with pitch angle and radial profile data

The probabilities of jumping the gaps as calculated in Section 6.2 can be used to estimate the effect of limiter shadowing on the baseline case. Some of the data can be understood qualitatively through this model, but the uncertainties are too large to allow a quantitative comparison.

The effect of limiter shadowing on the calculated pitch angle distributions is illustrated in Fig. 15, along with data for two aperture positions from Fig. 8. The two model curves are the baseline ORBIT code pitch angle distributions (Fig. 4) multiplied by the probability of missing the limiter as a function of pitch angle (assuming $E = 2.5$ MeV). The main effect is to shift the expected distribution to a higher pitch angle, since the probability of missing the limiter increases rapidly with pitch angle. For $r_{ap} = -0.5$ cm, the resulting 'ORBIT+shadowing' model distribution peaks close to the measured peak of the distribution at $\chi \approx 64°$. However, the data for $r_{ap} = -2.0$ cm peak at $\chi \approx 54°$, whereas the calculated pitch

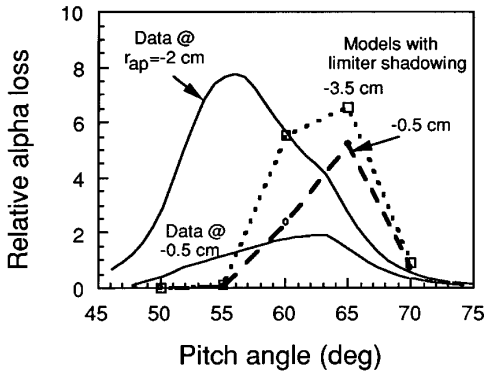

FIG. 15. Comparison of the calculated pitch angle distributions from a modified 'ORBIT+shadowing' model with the data for the baseline case. The peak in the modified model pitch distribution agrees well with the data for $r_{ap} = -0.5$ cm but not with the data for $r_{ap} = -2.0$ cm. The model pitch distribution is similar at $r_{ap} = -0.5$ cm for alpha particles in the range $E = 1.5$–3.5 MeV, but for $r_{ap} = -2$ cm there may be a contribution from 'confined' alpha particles at low pitch angle (not shown). The relative vertical scale between the data and the models is arbitrary.

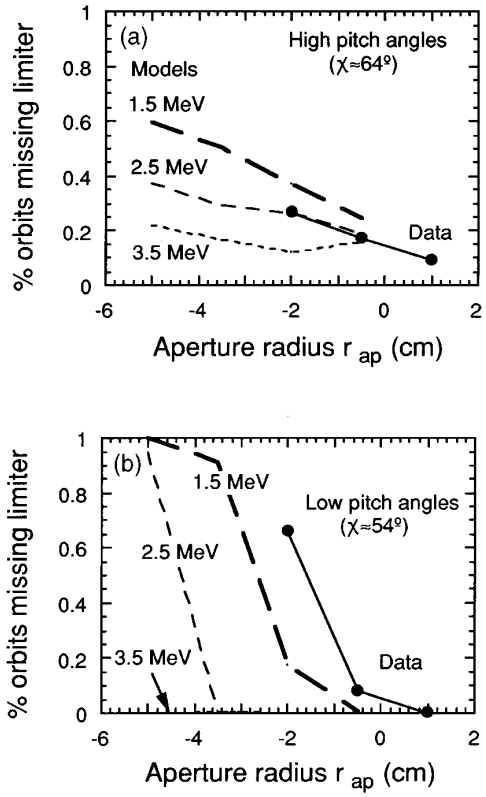

FIG. 16. Radial profiles of the data for the baseline case resolved into two separate pitch angle components ((a) and (b)), along with limiter shadowing models for each. (a) At high pitch angles ($\chi \approx 64 \pm 6°$), the radial profile of the data is similar to the calculations with ripple diffusion behind the limiter shadow for $E = 2.5$ MeV. For low pitch angles ($\chi \approx 54 \pm 6°$), the radial profile of the data is consistent with the collection of 'confined' alpha particles when the gap is effectively zero. For the vacuum model in this calculation, this zero gap condition occurs at an aperture radius of $r_{ap} = -4$ cm for $E = 2.5$ MeV, while the data suggest this actually occurs at $r_{ap} = -2$ cm. This difference is probably due to uncertainties in the magnetic fields in the vacuum region near the outer limiter.

distribution for $r_{ap} = -2.0$ cm, and even $r_{ap} = -3.5$ cm (as shown), still peaked near $\chi \approx 64°$. Therefore, a mechanism other than SRD must cause the observed low pitch angle peak at $\chi \approx 54°$ for the $r_{ap} = -2.0$ cm case.

To explore this comparison further, it is useful to decompose the measured pitch angle distribution into two components, as suggested by the data of Fig. 8; namely, one component centred at low pitch angles of $\chi \approx 54°$ and the other at high pitch angles of $\chi \approx 64°$, both with a width of $\pm 6°$. The resulting radial profiles of the data for the baseline case are compared with the radially resolved probability of missing the limiter in Fig. 16. For high pitch angles, the probability of missing the limiter increases as the aperture moves towards the plasma because the gap becomes smaller, and so a radial jump across the gap becomes more likely. The data for $\chi \approx 64°$ can be fairly well fitted by the SRD jump model for an alpha particle energy of $E \approx 2.5$ MeV. For the lower pitch angles, the increase in probability occurs only when the gap becomes zero, i.e. when orbits traced backwards from the aperture are not shadowed by the limiter. At $\chi = 54°$ this seems to require an energy of $E < 1.5$ MeV to fit the data, but the location of this boundary is uncertain owing to its dependence on the vacuum fields (Appendix). Thus, it is most likely that the dominant low pitch angle feature at $r_{ap} = -2$ cm is due to the collection of 'confined' alpha particles, which only occurs when the aperture is located far enough in that there is no limiter shadowing. The expected flux for this process is estimated in Section 6.4.

The good fit for the high pitch angles case in Fig. 16 suggests that the limiter shadowing model might help explain the total loss data versus $q(r)$ of

Fig. 7 for $r_{ap} = +1.0$ cm, all of which were at high pitch angles (Fig. 9). Qualitatively, there are two limiter shadowing effects which vary with plasma type: the size of the SRD jumps increases linearly with $q^{3/2}\rho$ (Eq. (4)), and the size of the gaps varies with the outer limiter q and the Shafranov shift. The first effect causes the jumps to decrease by ≈15% as B is lowered in the $q(a)$ scan and to increase by ≈40% as B is lowered in the ρ scan. Neither trend is in the direction of explaining the deviations of the data at $r_{ap} = +1.0$ cm from the scaled ORBIT model results of Fig. 7. And although the vacuum fields did vary with the type of plasma, the resulting limiter shadowing probabilities for the $r_{ap} = +1.0$ cm cases did not tend to explain the trends in the data. The uncertainties in the vacuum fields at the limiter and in the energy spectrum of the alpha particle loss are apparently too large to allow a quantitative explanation of the present data.

6.4. Finite gyroradius effects

One factor not taken into account in the limiter shadowing model above was the finite perpendicular gyroradius of the alpha particles, which for this experiment was in the range $\rho \approx 5$–11 cm. This is comparable to the size of the jumps and gaps in the guiding centre modelling, and so could potentially be important in determining the alpha particle flux to the detector near the shadow of the limiter.

Calculations of the limiter shadowing effect that included the finite gyroradius were done using a modified version of the Lorentz orbit code [14]. This version had magnetic fields taken from the full 2-D magnetic equilibrium for the baseline case (including vacuum fields), and a very accurate 3-D model of the limiter geometry. Orbits were started at the aperture location with a gyrophase angle within the narrow range (±2°) defined by the detector aperture pair (Section 3). The orientation of this gyrophase acceptance range was originally designed to avoid limiter shadowing as much as possible by collecting alpha particles only near the outermost major radial excursion of their gyro-orbits [17].

These calculations generally confirmed the simplified limiter shadowing picture described in Section 6.1. For example, the gap sizes, as calculated by this Lorentz code, decreased as the alpha particle energy and pitch angle decreased, as expected. However, the gaps were consistently $\Delta_r \approx 1$ cm smaller from the finite gyroradius code, as illustrated for the $E = 1.5$ MeV case in Fig. 13. It was also found that

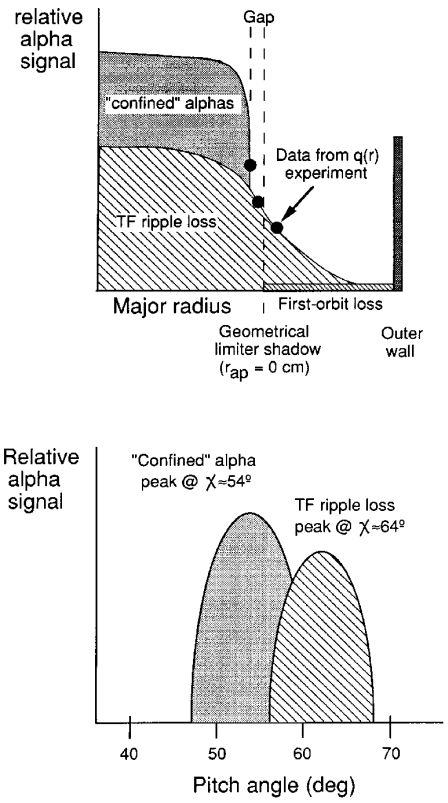

FIG. 17. Qualitative picture of the effects of limiter shadowing on alpha particle detection in this experiment. The TF ripple loss falls off in the limiter shadow with an e-folding length comparable to the radial step size for SRD. When the aperture is far enough inward it begins to collect 'confined' alpha particles, which need not have any radial diffusion to be detected. The measured pitch angle distributions represent a combination of these two mechanisms. The aperture was not far enough outward in this experiment for a significant first orbit loss component.

a single outer midplane limiter shadows all the alpha particle orbits for which any part of the gyro-orbit extends beyond $a_{lim} = 99$ cm, since each limiter has a toroidal extent that is larger than the toroidal length (≈20 cm) of a single gyro-orbit. In addition, since the vacuum field q is very large ($q \approx 25$) near the outer limiter (Appendix), nearly all the escaping alpha particle orbits can be blocked by any one of these outer limiters when the orbit crosses the outer midplane.

The small difference between the gaps calculated by the ORBIT and Lorentz codes is not due to the finite gyroradius, but is most likely due to the slightly different radial profiles of the vacuum fields and the

slightly non-circular flux surfaces used in this full 2-D equilibrium model compared with the ORBIT field model. This shows again that the structure of the vacuum fields is important for the gap and limiter shadowing calculations.

6.5. Estimate of expected absolute flux

Given the strong radial dependence of the measured alpha particle signals, the absolute alpha particle flux into the detector can only be understood by using some type of limiter shadowing model. Recall that the measured alpha particle collection fractions for the baseline case were estimated to be in the range from 10^{-7} to 10^{-6} (Fig. 5), i.e. the absolute alpha particle flux into the detector aperture varied from $\approx 10^{10}$ to 10^{11} alpha particles/s between $r_{ap} = +1.0$ cm and -2 cm for a typical DT neutron rate of $\approx 10^{17}$ n/s.

On the basis of the discussion in the preceding sections, a qualitative picture of the alpha particles collected by this detector is shown in Fig. 17. There are three components to the detected alpha particle loss:

(a) The radially diffusing alpha particles crossing the gap due to SRD, which are dominant only when the gap is slightly positive;

(b) The 'confined' alpha particles seen by the detector only when the gap is negative (Section 6.3);

(c) The first orbit loss to the limiter, which is significant only when the gap is positive and large.

The SRD is dominant only in a narrow radial region near the geometrical limiter shadow, where the radial jump due to SRD is comparable to the size of the gap, which was the location used for the present experiment.

An approximate a priori estimate of the absolute level of SRD-induced alpha particle loss collected by the detector aperture can be obtained from a combination of the global ripple loss, the limiter shadowing model and the detector and geometrical parameters,

$$F_{rip}(r) = P_{rip}(E,\chi) P_r(r,E,\chi) P_\theta(r,E,\chi) \times P_{gyro}(r,E,\chi). \quad (5)$$

Here $F_{rip}(r)$ is the alpha particle ripple loss collection fraction in the detector when its aperture is at a radius 'r', $P_{rip}(E,\chi)$ is the global probability for TF ripple loss as a function of the alpha particle loss energy and pitch angle (e.g., taken from ORBIT calculations such as those shown in Fig. 4), $P_r(r,E,\chi)$ is the probability for an alpha particle ripple loss orbit to be lost within the radial acceptance range of the detector aperture (≈ 0.07 cm), $P_\theta(r,E,\chi)$ is the probability for an alpha particle ripple loss orbit to be within the poloidal acceptance range of the detector aperture and $P_{gyro}(r,E,\chi)$ is the probability that an alpha particle ripple loss orbit entering the front aperture of the detector has a gyrophase that also passes through the back aperture of the detector. In general, each of these geometrical factors depends on the energy and pitch angle of the alpha particles, so the total ripple loss at a given 'r' is the sum over all relevant (E,χ).

The simplest estimate for the alpha particle collection fraction induced by SRD for an aperture position just outside the limiter shadow can be made by assuming that the global ripple loss ($\approx 7\%$) is radially distributed uniformly over a width equal to the two SRD 'jumps' on the last confined alpha particle orbit (≈ 6 cm), poloidally distributed uniformly over 30° below the outer midplane (Fig. 4), and uniformly distributed in gyrophase angle at the aperture. For these assumptions, $P_{rip} = 7 \times 10^{-2}$, $P_r = (0.07\text{ cm})/(6\text{ cm}) \approx 1 \times 10^{-2}$, $P_\theta = (0.2\text{ cm})/(50\text{ cm}) \approx 4 \times 10^{-3}$ and $P_{gyro} \approx (0.07\text{ cm})/(1\text{ cm}) \approx 7 \times 10^{-2}$; thus, $F_{rip} \approx 2 \times 10^{-7}$. This simple estimate is close to the estimated alpha particle collection fraction of $F \approx 3 \times 10^{-7}$ near $r_{ap} = -0.5$ cm (Fig. 5), but this should be considered only as an order of magnitude agreement.

The most uncertain part of this estimate is the radial profile of the probability distribution of TF ripple loss in the shadow of the limiter. As discussed in Section 6.3, this function depends sensitively on the alpha particle energy and pitch angle, as well as the magnetic field structure in the vacuum, which determines the gap sizes. Even for a fixed gap size the radial profile depends not only on the average size of the radial jumps but also on the distribution of jump sizes, which depends on the degree to which the last confined alpha particle orbits are stochastic [17].

The expected TF ripple loss can alternatively be estimated by comparison with the first orbit loss, which can be calculated absolutely using the Lorentz orbit code. The calculated ripple loss at the poloidal angle of the detector is locally a factor of ≈ 3 higher than the first orbit loss (Fig. 4), and the radial extent of the first orbit loss behind the limiter shadow is larger owing to its effectively large 'jump' at the banana tip, which causes the loss to be distributed over a larger poloidal angle. Estimating this jump to be ≈ 3 times larger than that for TF ripple loss, and assuming the same probability of gyrophase

detection, the estimated ripple loss just behind the limiter shadow is ≈10 times the calculated first orbit loss into the detector, i.e. similar to the above estimate.

When the aperture is effectively inside the limiter shadow the detector can collect alpha particle orbits with low pitch angles that would normally be confined until thermalized, except for the presence of the detector itself [12]. The probability of being detected is then the first orbit collection efficiency multiplied by the average number of poloidal transits made before the orbit intersects the ≈6 cm wide detector shaft [17]. The latter is typically $(2\pi a/6\ \text{cm}) \approx 100$, so that the collection fraction for such 'confined' alpha particles could be up to 100 times the first orbit loss level, i.e. qualitatively consistent with the level found for the $r_{\text{ap}} = -2$ cm aperture position for the baseline case. Such 'confined' alpha particles would tend to be lost soon after birth and at low pitch angles, where the shadowing effect is smallest. It should be emphasized that this class of particles is expected even without any SRD, since at low pitch angles these orbits can have banana tips in the SRD-free region.

These are clearly only order of magnitude estimates of the absolute flux, and so are clearly not useful for interpreting the relatively small differences between the results for different $q(r)$ found in this experiment. A significantly better limiter shadowing model would be needed to calculate the relative alpha particle flux versus detector position before these measurements can be understood quantitatively. Some potential improvements are discussed in Section 7.

7. DISCUSSION

This experiment has found that the alpha particle loss to a detector near the outer midplane depends strongly on the $q(r)$ profile and the alpha particle gyroradius in TFTR DT plasmas. However, the measured alpha particle loss is not simply proportional to the calculated global alpha particle ripple loss, as had been expected initially, but appears to depend sensitively on the details of the limiter shadowing process. Some features of the data were qualitatively explained by a simplified limiter shadowing model, but a quantitative understanding of the data requires a considerably improved ripple loss model and a much better knowledge of the vacuum magnetic fields and of the energy distribution of the escaping alpha particles.

7.1. Relationship to other experiments

It is interesting to compare the difficulties encountered in the present article with the results from previous fast ion loss experiments in TFTR and other tokamaks. Techniques based on measuring confined fast ions using triton burnup, neutron production or charge exchange have different problems of interpretation [4–9].

In TFTR, the DT alpha particle loss to a detector at the bottom of the vessel was successfully interpreted using the first orbit loss model without considering the effect of limiter shadowing [14]. This was possible since the aperture was located only ≈1 cm behind the limiter shadow, and was intentionally designed such that all the alpha particle loss orbits were unobstructed by the limiter on their first transit from the plasma to the detector. However, an anomalous alpha particle loss component with low energy was recently measured by a foil deposition detector when it was located ≈1 cm above the limiter shadow at this poloidal location [28], and similar difficulties in interpreting the limiter shadowing effect were also encountered there.

Previous studies of DD fusion product loss at the outer midplane of TFTR also considered the importance of the limiter shadowing effect on the interpretation made [12]. The qualitative features of the DD data were similar to those of the DT data described here and in Ref. [13]. However, the earlier DD data were taken for aperture positions far behind the limiter shadow ($r_{\text{ap}} \approx +5$–10 cm), so that a direct comparison could be made with the first orbit loss. A measurement of the shadowing effect was also made using a movable obstacle, allowing a clearer inference of the radial diffusion rate and comparison with the stochastic diffusion model. Neither of these experiments was possible in DT, owing to increased background levels and removal of the second movable probe.

The only other experiments that directly measured fast ion loss due to stochastic ripple diffusion (also called banana drift diffusion) were done using an infrared TV camera in JT-60U [5, 29], where the wall heating due to ICR minority heating and NBI ion loss was compared with the results using a ripple loss code. This measurement technique averages over pitch angle, energy and radial co-ordinate, but has a much better spatial coverage than the scintillator detector in TFTR. Despite the relatively smooth outer wall of JT-60U, the original measurements [5] could not be quantitatively interpreted, owing to a slight misalignment of the outer wall tiles (≈0.2 cm),

which caused localized heat deposition at the tile edges. Later measurements [29] were more successful in comparing the total NBI heat flux to the outer wall with the banana drift diffusion calculated by the OFMC code (similar to the ORBIT code). The spatial profile of the banana drift ripple loss could be roughly explained by the OFMC calculations on a scale of ≈10 cm, but was not explained on a smaller scale (≈0.1–1 cm).

The conclusion from this comparison with other experiments is that the stochastic ripple loss of fast ions to the wall has never been quantitatively understood on a scale comparable to the detector size of the TFTR experiment, mainly because the limiter shadowing effect cannot be accurately calculated at that small scale. The ripple trapped loss of fast ions appears to be somewhat better understood [7, 30, 31], since the location of this loss channel is mainly determined by the shape of the TF ripple wells and by the ripple induced wobble in the outermost magnetic field lines, and not by shadowing due to remote limiters.

7.2. Potential improvements in modelling

The most direct way to obtain a quantitative understanding of the present experimental data would be to model the collisional ripple loss accurately enough to calculate the local flux into the detector aperture. In principle this can be done by putting the full 3-D geometry of the detector and limiters into a Monte Carlo guiding centre code such as ORBIT. But to be useful for interpreting the pitch angle and energy resolved data, these code results would require at least ≈100 particles to be collected by the detector. Given the detector collection efficiency of $\approx 10^{-7}$ (Fig. 5), this implies that $\approx 10^{9}$ alpha particles need to be followed for about one slowing down time. This would require $\approx 10^{6}$ times more computing power than has been applied to the present modelling, and so is completely impractical.

A more efficient method might be to use the ORBIT code to follow alpha particle orbits backward from the detector in time into the plasma to their birth energy, appropriately weighting the results with the alpha particle source profile. This could improve the estimate of the expected limiter shadowing probability versus energy and pitch angle, although it is not yet clear how the absolute flux could be calculated in this way. Since the probability of missing the limiter decreases rapidly with the number of transits (e.g., when ≈10% miss after one poloidal transit, <0.1% miss after 1000 poloidal transits), a large number of orbits ($\approx 10^{4}$) still need to be launched at each pitch angle to simulate the detected signal. This was attempted in Ref. [20] with some qualitative success using a simplified orbit and magnetic geometry. It is also likely that finite gyroradius effects also need to be evaluated to have confidence in the predictions of such a guiding centre model.

A practical difficulty with this approach is that the results will still be sensitive to the limiter geometry and vacuum magnetic fields. For example, the uncertainty of the outer limiter radii in TFTR was at best ±0.3 cm and was probably larger by the end of TFTR operation. This introduces a significant uncertainty in the calculated ripple loss, since the radial e-folding length of alpha particle loss in the shadow of the limiter is typically ≈1–2 cm. The limiter shadowing effect is also very sensitive to the structure of the vacuum flux surfaces, as discussed in the Appendix. For example, an uncertainty of ±1 cm in the magnitude of the ≈20 cm inward Shafranov shift of the magnetic flux surface passing through the detector causes another ±1 cm uncertainty in the limiter shadowing effect.

Finally, the ripple loss physics and the limiter shadowing effect also depend sensitively on the alpha particle energy through the shape of the banana orbits, so a precise measurement of the alpha particle energy spectrum is needed for a quantitative verification of the SRD mechanism. Such a measurement could also check the expected collisional ripple loss spectrum, and potentially distinguish this from 'confined' alpha particles, which should be lost near the birth energy. However, the present instrumental resolution of ±1 MeV probably needs to be ≈10 times better for this purpose.

7.3. Conclusions

The result of this experiment was that the alpha particle loss measured near the outer midplane wall of TFTR did depend strongly on the $q(r)$ profile in the plasma. For example, at a fixed detector aperture location, the measured alpha particle collection fraction varied by about a factor of 2 with variations in the $q(r)$ profile at constant $q(a)$, and by a similar factor with variations in $q(a)$. However, the alpha particle signal also varied strongly with the detector aperture location for all cases, with a typical radial e-folding length of ≈1–2 cm.

Guiding centre code simulations alone were not able to quantitatively interpret these results in terms of the stochastic ripple diffusion model. The main difficulties in the analysis of the present experiment were

that the escaping alpha particle banana orbits which were undergoing stochastic ripple diffusion were shadowed by the limiter near the outer midplane, and that diffusion behind this limiter had the small radial step size characteristic of SRD. This made the location of the alpha particle loss highly dependent on the limiter and detector geometry, and also on the vacuum magnetic field structure, which determined the orbit shape near the outer limiter. Consequently, the calculation of alpha particle loss to the very small detector aperture was quite uncertain.

For future DT tokamak reactors such as ITER, this result implies that the local alpha particle heat loads on the wall due to stochastic ripple diffusion can probably not be reliably predicted, even though the large scale pattern of alpha particle ripple loss on the wall can be estimated from Monte Carlo codes [29, 32]. This is a potential engineering problem, since overheating of even centimetre-scale sections of the first wall could cause impurity influx or wall damage. The main uncertainty in these calculations is due to slight misalignments of the first wall and to a lack of knowledge, or a variability, of the vacuum magnetic flux surfaces near the outer limiters.

Appendix

SENSITIVITY OF SRD LOSS TO VACUUM FIELDS

As pointed out by Goloborod'ko et al. [33], the magnetic fields in the vacuum region outside the plasma but inside the limiter are difficult to calculate analytically. The only available solutions for TFTR come from an EFIT equilibrium reconstruction [34], which includes the MSE data on $q(r)$ inside the plasma and the coil currents of the ohmic heating and equilibrium field coil systems. A general feature of the equilibria for this experiment is that $q(r)$ increases much more rapidly in the vacuum region than would be expected from a cylindrical model in which $q(r) \propto (r/a)^2$, and the shift becomes very negative for flux surfaces near the limiter. Typical values of q and the Shafranov shift near the outer limiter midplane for these plasmas were $q_{\rm lim} = 25 \pm 5$ and -17 ± 3 cm, respectively, for $q(a) \approx 6.5$ and zero shift at the plasma edge.

These vacuum fields are important in determining the shape of the marginally confined alpha particle orbits in TFTR [35], and so strongly affect the size of the 'gap' between the last confined orbit and the outer limiter. An example of the sensitivity of the calculated gaps to the assumed vacuum fields for the baseline plasma case is given in Ref. [17], where the value of q and the shift were kept constant at the plasma edge but varied at the limiter. For these examples the gap decreased ≈1 cm for each 1 cm inward shift of the flux surface at the outer wall, i.e. the gap size is uncertain by about the same amount as the shift of this flux surface. The gap also decreases as the value of $q_{\rm lim}$ decreases, since the outward orbit shift decreases with decreasing edge q. Thus, the calculated gaps have a significant uncertainty; for example, the EFIT baseline model with $q_{\rm lim} = 25$ and a shift of −17 cm at the outer midplane limiter implies a gap of 5.3 cm for an $E = 2.5$ MeV, $\chi = 60°$ alpha particle at $r_{\rm ap} = 0$ cm, whereas for a shift of −20 cm the gap is ≈7 cm, and for $q_{\rm lim} = 20$ the gap is ≈4 cm. The uncertainties of the limiter flux surface shift and q are not well characterized, but are very likely to be within these ranges.

The sensitivities of the limiter shadowing probability to q and the shift at the outer limiter are also illustrated in Ref. [17]. As expected from the variation of the gaps with these variables, the probability of missing the limiter, as described in Section 6.1, depends sensitively on the assumed q and shift at the outer limiter. For example, this probability changes from ≈10% for the baseline case (with $q_{\rm lim} = 25$ and a shift of −17 cm) to ≈20% for $q_{\rm lim} = 18$ and a shift of −21 cm. Again, these are likely to be within the range of uncertainty of the edge vacuum fields in TFTR.

ACKNOWLEDGEMENTS

We are grateful to M. Bell, R. Boivin, C.S. Chang, R.J. Hawryluk, D.W. Johnson, G. LeMunyan, K.M. McGuire, D.K. Owens, J. Schivell, J.D. Strachan, K.M. Young and M. Zarnstorff for their contributions to this experiment. We particularly thank our colleague V. Yavorskij of the Ukrainian Institute of Nuclear Research for pointing out the effect of vacuum magnetic fields on alpha particle loss orbits in TFTR, and S. Wang of the Academia Sinica for his previous calculations on the limiter shadowing effect. This work was supported by USDOE Contract No. DE-AC02-76-CH03073.

REFERENCES

[1] GOLDSTON, R.J., WHITE, R.B., BOOZER, A., Phys. Rev. Lett. **47** (1981) 647.
[2] WHITE, R.B., GOLDSTON, R.J., REDI, M.H., BUDNY, R.V., Phys. Plasmas **3** (1996) 3043.
[3] REDI, M.H., WHITE, R.B., BATHA, S.H., LEVINTON, F.M., McCUNE, D.C., Phys. Plasmas **4** (1997) 4001.
[4] HEIDBRINK, W.W., SADLER, G., Nucl. Fusion **34** (1994) 535.
[5] TOBITA, K., et al., Nucl. Fusion **35** (1995) 1585.
[6] SADLER, G., et al., Nucl. Fusion **35** (1995) 1609.
[7] BASIUK, V., et al., Nucl. Fusion **35** (1995) 1593.
[8] DUONG, H.H., et al., Nucl. Fusion **37** (1997) 271.
[9] TOBITA, K., et al., Nucl. Fusion **37** (1997) 1583.
[10] RUSKOV, E., et al., in Alpha Particles in Fusion Research (Proc. 5th IAEA Tech. Comm. Mtg Abingdon, 1997), JET Joint Undertaking, Abingdon (1997) 165.
[11] BOIVIN, R., ZWEBEN, S.J., WHITE, R.B., Nucl. Fusion **33** (1993) 449.
[12] BOIVIN, R., ZWEBEN S.J., Phys. Fluids B **5** (1993) 1559.
[13] ZWEBEN, S.J., et al., Nucl Fusion **35** (1995) 1445.
[14] ZWEBEN, S.J., et al., Nucl. Fusion **35** (1995) 893.
[15] BATHA, S., et al., Nucl. Fusion **35** (1995) 1463.
[16] HIRSHMAN, S., et al., Phys. Plasmas **1** (1994) 2277.
[17] ZWEBEN S.J., et al., Effects of $q(r)$ on the Alpha Particle Ripple Loss in TFTR, Rep. PPPL-3264, Princeton Plasma Phys. Lab., NJ (1997), available on the WWW at http://www.pppl.gov/
[18] DARROW, D.S., et al., Rev. Sci. Instrum. **66** (1995) 476.
[19] BOIVIN, R.L., KILPATRICK, S., MANOS, D., ZWEBEN, S.J., Rev. Sci. Instrum. **63** (1992) 4562.
[20] WANG, S., ZWEBEN, S.J., Model of Alpha Particle Diffusion in the Outer Limiter Shadow of TFTR, Rep. PPPL-3186, Princeton Plasma Phys. Lab., NJ (1996).
[21] REDI, M.H., et al., Nucl. Fusion **35** (1995) 1191.
[22] REDI, M.H., et al., Nucl. Fusion **35** (1995) 1509.
[23] VON GOELER, S., et al., Rev. Sci. Instrum. **68** (1997) 548.
[24] BOOK, D.L., NRL Plasma Formulary, NRL/PU/6790–94-265, Naval Research Lab., Washington, D.C. (1994).
[25] RAMSEY, A.T., et al., Rev. Sci. Instrum. **68** (1997) 632.
[26] ZWEBEN, S.J., et al., Phys. Plasmas **1** (1994) 1469.
[27] TAKAHASHI, H., Fusion Eng. Des. **34&35** (1997) 89.
[28] HERRMANN, H.W., et al., Nucl. Fusion **37** (1997) 293.
[29] IKEDA, Y., et al., Nucl. Fusion **36** (1996) 759.
[30] TOBITA, K., et al., Phys. Rev. Lett. **69** (1992) 3060.
[31] TUSZEWSKI, M., ROUBIN, J.P., Nucl. Fusion **28** (1988) 499.
[32] CHENG, C.Z., et al., in Fusion Energy 1996 (Proc. 16th Int. Conf. Montreal, 1966), Vol. 2, IAEA, Vienna (1997) 953.
[33] GOLOBOROD'KO, V., et al., Nucl. Fusion **35** (1995) 1523.
[34] LAO, L.L., et al., Nucl. Fusion **25** (1985) 1611.
[35] YAVORSKIJ, V., Ukrainian Institute for Nuclear Research, Kiev, personal communication, 1997.

(Manuscript received 29 October 1997
Final manuscript accepted 27 January 1998)

E-mail address of S.J. Zweben: szweben@pppl.gov

Subject classification: F2, Te; F3, Te